Infrared-modulated photoluminescence spectroscopy: From wide-band coverage to micro-area and high-throughput scanning imaging*

SHAO Jun[1,2], CHEN Xiren[1,3], WANG Man[1,4], LU Wei[1,2]

[1]*National Laboratory for Infrared Physics, Shanghai Institute of Technical Physics, Chinses Academy of Sciences, Shanghai 200083, China*

[2]*School of Physics and Optoelectronic Engineering, Hangzhou Institute for Advanced Study, University of Chinese Academy of Sciences, Hangzhou 310024, China*

[3]*National Key Laboratory of Infrared Detection Technologies, Shanghai Institute of Technical Physics, Chinese Academy of Sciences, Shanghai 200083, China*

[4]*University of Chinese Academy of Sciences, Beijing 100049, China*

Abstract

Photoluminescence (PL) spectroscopy has been widely used in the ultraviolet-near-infrared spectral range for over seventy years since its early reporting in the 1950's, because it not only reveals the electronic structure information about band gap and impurity energy levels of semiconductor materials, but also serves as an efficient tool for analyzing interfacial structures, carrier lifetime, and quantum efficiency. However, in the infrared band beyond about 4 μm, the study of PL spectroscopy has been limited for decades due to strong thermal background interference, weak PL signals and low detection capability. In this review, a traditional Fourier transform infrared (FTIR) spectrometer-based PL spectroscopic method is introduced, and a continuous-scan FTIR spectrometer-based double-modulation PL (csFTIR-DMPL) method is briefly described with its limitations emphasized, which was proposed in 1989 for breaking through the dilemma of the infrared band and developed continuously in the later more than 20 years. Then, a step-scan FTIR spectrometer-based infrared modulated PL (ssFTIR-MPL) method we reported in 2006 is analyzed with highlights on its advantages of anti-interference, sensitivity, and signal-to-noise ratio. The effectiveness demonstration and application progress of this method in many research groups around the world are listed. Further developments in our group in the recent years are then summarized of wide-band, high-throughput scanning imaging and spatial micro-resolution infrared modulated PL spectroscopic experimental systems, and the technological progresses are demonstrated of infrared-modulated PL spectroscopy from 0.56–20 μm visible-far-infrared broadband coverage to >1000 high-throughput spectra imaging and ≤ 2–3 μm spatial micro-resolution. Typical

* The paper is an English translated version of the original Chinese paper published in *Acta Physica Sinica*. Please cite the paper as: SHAO Jun, CHEN Xiren, WANG Man, LU Wei, Infrared-modulated photoluminescence spectroscopy: From wide-band coverage to micro-area and high-throughput scanning imaging. *Acta Physica Sinica* 2025, 74(1): 017801. doi: 10.7498/aps.74.20241491

achievements of collaborative research in our group are enumerated in the visible-far-infrared semiconductor materials of dilute nitrogen/dilute bismuth quantum wells, HgCdTe epitaxial films, and InAs/GaSb superlattices. The results presented demonstrate the advancement of infrared modulated PL spectroscopy and the effectiveness of the experimental systems, and foresee further application and development in the future.

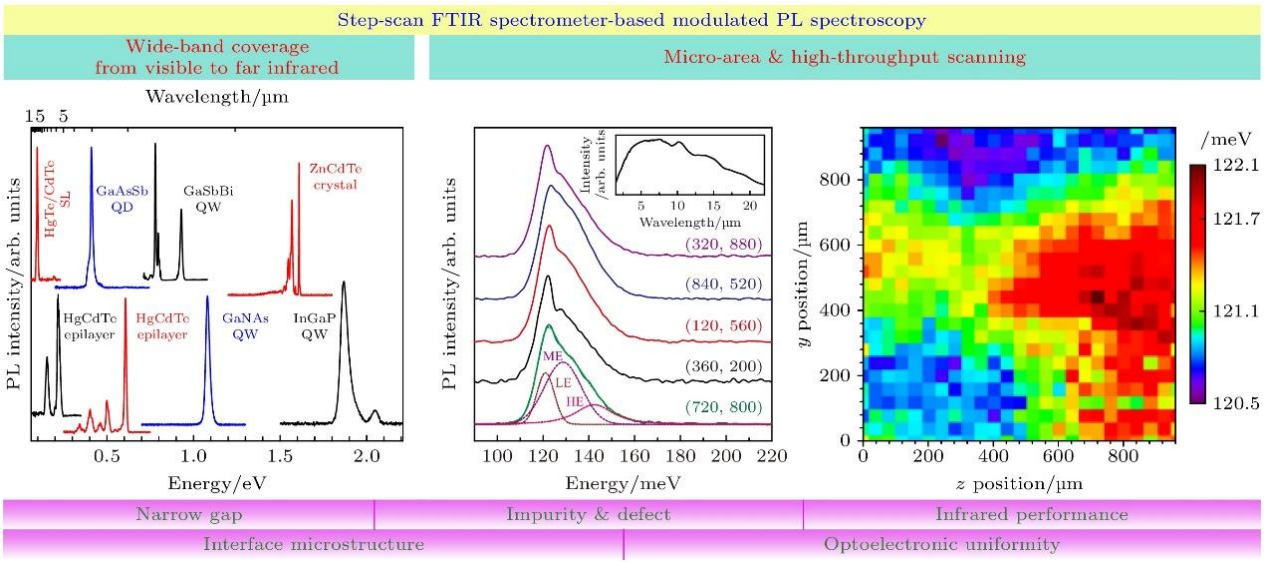

Keywords: photoluminescence, Fourier transform infrared spectrometer, step scan, semiconductor

PACS: 78.55.–m, 07.57.Ty, 74.25.nd, 61.72.uj

doi: 10.7498/aps.74.20241491

cstr: 32037.14.aps.74.20241491

Table of contents

1. Introduction

Optical spectroscopy is one of the few important ways for human beings to understand the objective world. Optical spectroscopy and its technological development have always attracted much attention and played a decisive role in enhancing the understanding of material science. As a classical and effective method for nondestructive testing of semiconductor materials, photoluminescence (PL) spectroscopy has the advantages of being simple and nondestructive, requiring only a small amount of material samples, mainly providing information about minority carrier properties, and forming an effective supplement to electrical characterization methods. It is widely used in the study of ultraviolet-near-infrared optical properties of wide-gap semiconductors such as III-V group semiconductors and nanomaterials such as carbon nanotubes. It can not only reveal the electronic band structure information of materials, such as band gap and band edge states, but also be used to study impurities, deep level defects, interfaces, and infer lifetime, diffusion length, and quantum efficiency[1-5] Thanks to the advantages of multiplex and high-throughput of Fourier transform infrared (FTIR) spectrometer, FTIR-PL spectroscopy has been successfully applied[6–8] in areas where traditional dispersive spectroscopy measurement is almost impossible.

Infrared optoelectronic materials and devices possess both fundamental physical problems and important application scenarios. For example, the infrared focal plane array (IRFPA) detector based on semiconductor materials such as HgCdTe and InAs/GaSb type-II superlattices (SLs) is the core device of modern information equipment, its performance improvement is limited by the photoelectric properties of the material and its microscale uniformity infrared focal plane array[9,10]; infrared materials based on quantum regulation and nanostructure have attracted great attention in recent years, and the researches on basic physics of related semiconductor materials and application of single photon devices develop continuously toward quantum/nano wires, quantum dots (QDs), and single-point defects.[11-13] This requires the PL spectroscopic method to possess both long-wave infrared band applicability and micrometer-scale spatial resolution capability.

However, the expansion of the applicable range of PL spectroscopy into the infrared band is restricted by mechanistic limitations. In the infrared of beyond a wavelength of approximate 4 μm, the room-temperature background radiation is much stronger than the PL signal of semiconductor materials, and the detection sensitivity of the available infrared photodetectors is reduced by orders of magnitude compared to that of the visible-band counterparts. This has led over a fairly long period past to very limited successful research even on conventional large-spot randomly excited PL measurements. To address this, a continuous-scan FTIR spectrometer-based double-modulated PL

(csFTIR-DMPL) spectroscopic method has been developed based on a continuous-scan FTIR spectrometer since 1989 [14-17], and PL spectroscopic analysis has been conducted on narrow-gap semiconductors such as HgCdTe [18-20]. Nevertheless, due to the fact that the continuous-scan mode of the FTIR spectrometer hinders the effective separation of the Fourier transform frequency and the excitation-light modulation frequency, the csFTIR-DMPL spectroscopic method does hence suffered fundamental limitations: even when the spectral resolution is not high (such as 8 cm^{-1}) and the single-spectra measurement time is on the order of hours, it is still difficult to obtain a high signal-to-noise ratio (SNR) PL spectrum suitable for quantitative line-shape analysis [15]. This severely limits its scope of application.

To address the actual needs of spatial resolution, the micro-photoluminescence (micro-PL, μPL) spectroscopic technology has attracted extensive attention. Commercial μPL spectrometers based on monochromator light dispersion and single-channel/linear/area array detectors can cover an applicable wavelength range from ultraviolet to near-infrared (0.19–1.6 μm) with an excitation light spots being smaller than 10 μm, and significant progress has been made in spatial resolution capabilities, materials of different dimensions and their impurities/defects, and the mechanisms of optoelectronic devices[21–24]. Nevertheless, due to the inherent limitations of the monochromator itself, the μPL spectroscopic technology is basically limited to the ultraviolet-near-infrared range with wavelengths of shorter than 1.6 μm, and cannot operate in the infrared of wavelength beyond approximate 3 μm.

In response to these needs and challenges, we developed a step-scan FTIR spectrometer-based modulated PL (ssFTIR-MPL) spectroscopic method[25], which significantly enhances spectral detection sensitivity and SNR[26–30]. We explored wide-band ssFTIR-MPL, high-throughput scanning imaging ssFTIR-MPL, and spatial micro-area resolution ssFTIR-μPL spectroscopic methods, by which we expand the applicable infrared bands and strengthen high-throughput spatial resolution and scanning imaging capabilities. The ssFTIR-MPL method has been successfully replicated by many research groups world-wide, and the ssFTIR-μPL and high-throughput scanning imaging ssFTIR-MPL methods have demonstrated technical advantage and played an active role in applied research. In the following, we will briefly describe the principle of FTIR-PL spectroscopic method, introduce the ssFTIR-MPL spectroscopic method, and wide-band and micro-area high-throughput spectroscopic methods, and summarize typical application cases, and forecasts the future development prospects of applications.

2. Fundamentals of FTIR-PL spectroscopic method

The instrument basis of FTIR-PL spectroscopy is an FTIR spectrometer, and the measurement principle of FTIR-PL spectrum is as shown in Fig. 1(a). The external laser pumps the sample and generates PL signal, the external optical path of the spectrometer (red dotted box) collects part of the PL signal and feeds it into the spectrometer, so that the Fourier modulation is realized by the moving-mirror scanning of the interferometer, and then the PL signal is received by the detector. The detector completes the photoelectric conversion, and the interferogram generated by the Fourier modulation is recorded through data acquisition and processing unit as[25]:

$$I_{\mathrm{cs}}^{\mathrm{d}}(\delta) = I_{\mathrm{PL}}(\delta) + I_{\mathrm{He-Ne}}(\delta) + I_{\mathrm{thermal}}(\delta), \tag{1}$$

where δ represents the optical path difference (in the unit of cm), which is the time function of the moving-mirror speed u, $\delta(t)=2ut$; $I_{\mathrm{PL}}(\delta)$ represents the interferogram of the PL signal to be measured, $I_{\mathrm{He\text{-}Ne}}(\delta)$ comes from the interference of the internal (He-Ne) laser of the interferometer , and $I_{\mathrm{thermal}}(\delta)$ is introduced by the environmental thermal background radiation.

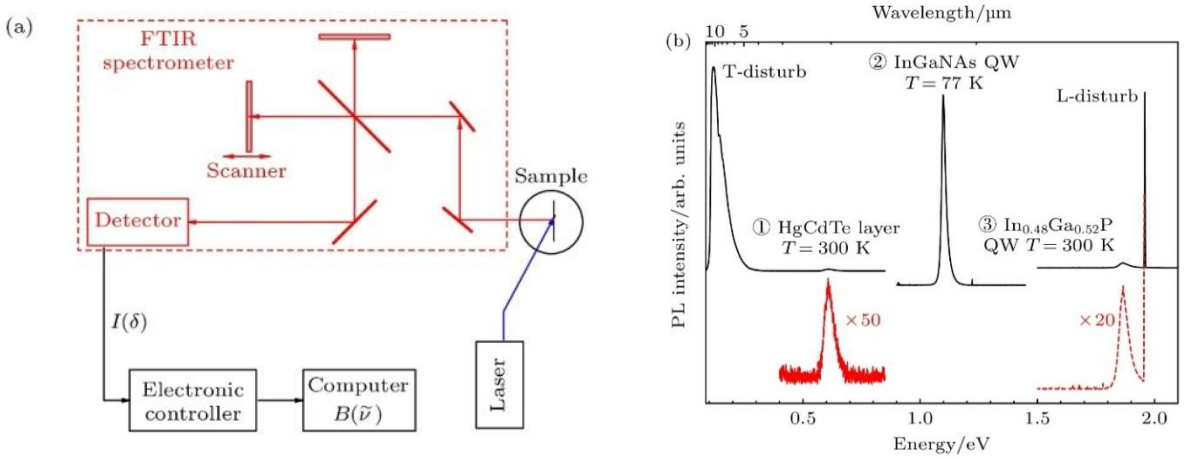

Figure 1. (a) Schematic of a FTIR-PL spectroscopic system. (b) PL spectra in different spectral bands in a wavelength range of about 0.6−12 μm from different semiconductors of ① HgCdTe epilayer, ② InGaNAs/GaAs quantum well (QW), and ③ InGaP/AlGaInP QW, black lines for measured data, red dashes for partially zoomed-in.

As the key information of a PL signal is reflected in the frequency/energy domain, the interferogram needs to be processed by inverse Fourier transform to obtain the spectrum $B(\tilde{\nu})$:

$$B_{\mathrm{RS}}(\tilde{\nu}) = \int_{-\infty}^{\infty} I_{\mathrm{RS}}^{\mathrm{d}}(\delta)\cos(2\pi\tilde{\nu}\delta)\,\mathrm{d}\delta = B_{\mathrm{PL}}(\tilde{\nu}) + B_{\mathrm{He-Ne}}(\tilde{\nu}) + B_{\mathrm{thermal}}(\tilde{\nu}),$$

$$\tilde{\nu}\delta = 2u\tilde{\nu}t = f_{\tilde{\nu}}^{\mathrm{cs}}t, \tag{2}$$

where $\tilde{\nu}$ represents energy (in the unit of cm^{-1}). It is clear that the PL spectrum obtained may contain the interferences from the internal (He-Ne) laser of the spectrometer and/or the ambient thermal background. As aforementioned, the optical path difference δ is a function of time of the moving mirror velocity u, a Fourier frequency $f_{\tilde{\nu}} = 2u\tilde{\nu}$ is hence introduced in here.

Typical experimental PL spectra are as shown in the Fig. 1(b). The PL spectrum as indicated by ① is of a HgCdTe epitaxial film in the mid-infrared band, the upper solid line is the measured result, which shows a strong peak at about 0.12 eV (or equivalently, at wavelength of about 10 μm) due to the thermal background radiation at room temperature; the lower (red) dotted line is the partially zoomed-in with a magnification of 50, which shows the *real* PL spectral signal from the measured sample with a very poor SNR. The PL spectrum as indicated by ② is of an InGaNAs/GaAs single quantum well (QW) sample in the near infrared band, which manifests only one unique spectral feature in the energy range of 0.95−1.20 eV (or equivalently, in a wavelength range of 1.03−1.30 μm). The PL spectrum as indicated by ③ is from an $In_{0.48}Ga_{0.52}P$/AlGaInP QW in the red band, of which the upper solid line is the measured result, which shows a broad spectral peak between 1.8 and 2.0 eV, together with a very sharp and strong line on its high energy side; the lower (red) dotted line is the partially zoomed-in with a magnification of 20. Combined with the sample and experimental conditions, it is inferable that the sharp and strong line corresponds to the He-Ne laser line, which is due to the interference of the He-Ne laser of the interferometer (of the FTIR spectrometer). The results show that in the bands covering the internal laser (600−700 nm) and/or environmental thermal background radiation (generally 5−15 μm), the conventional FTIR-PL spectroscopic method will inevitably be disturbed, and even become impossible for effective measurement[24].

3. Infrared modulation PL spectroscopic methods and experimental systems

3.1 ssFT-MPL spectroscopic method

The basic optical path of the ssFTIR-MPL spectroscopic method is as shown in Fig. 2(a)[25]. The moving mirror of the FTIR spectrometer is in the step-scan mode. The intensity-modulated external laser irradiates the semiconductor sample to generate PL signal, the latter passes through the interferometer and is then focused onto the detector, which realizes photoelectric conversion and outputs an interferogram as [25]:

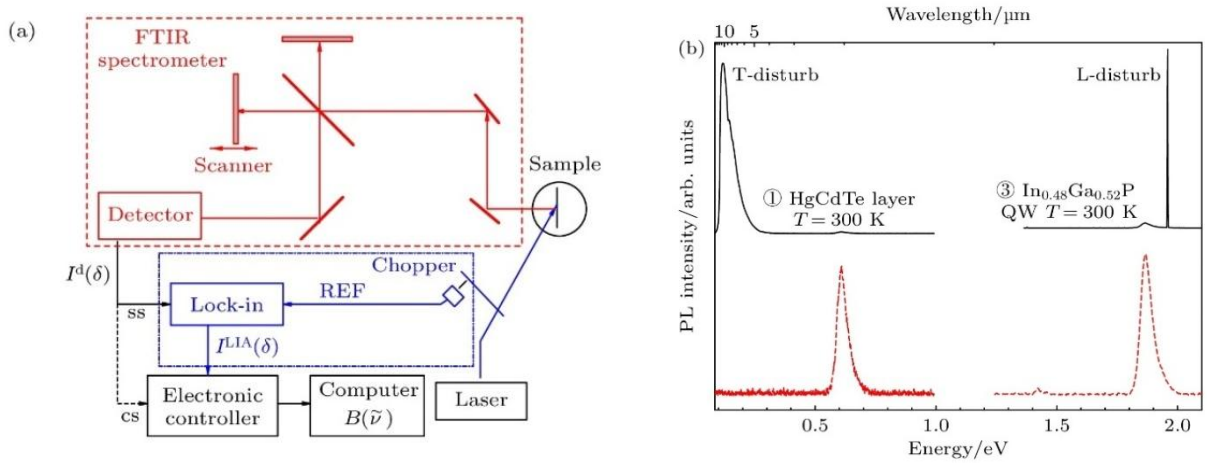

Figure 2. (a) Schematic of the ssFTIR-MPL spectroscopic system[25]. (b) PL spectra in different spectral bands from semiconductors of ① HgCdTe epilayer, and ③ InGaP/AlGaInP quantum well (QW), black lines by FTIR-PL, and red dashes by ssFTIR-MPL methods.

$$I_{\mathrm{ss}}^{\mathrm{d}}(\delta) = I_{\mathrm{PL}}(\delta)\sin(2\pi f_{\mathrm{m}} t + \theta_{\mathrm{PL}}) + I_{\mathrm{He-Ne}}(\delta) + I_{\mathrm{thermal}}(\delta). \tag{3}$$

For the step-scan mode, the sampling light path difference δ is not continuously time-varying, and the corresponding Fourier frequency is zero, that is, $f_{\tilde{\nu}}^{\mathrm{cs}} = 2u\tilde{\nu}$. The output signal of the detector is preamplified and phase-sensitively detected by a lock-in amplifier (LIA) to filter out all f_{m} and $2\,f_{\mathrm{m}}$ components of the signal, and becomes

$$I_{\mathrm{ss}}^{\mathrm{LIA}}(\delta) = \frac{v_{\mathrm{ref}} K^{\mathrm{LIA}}}{2} I_{\mathrm{PL}}(\delta)\cos(\theta_{\mathrm{PL}} - \theta_{\mathrm{ref}}). \tag{4}$$

The equation does no longer contain the interference terms of internal laser and environmental thermal background, only the *real* PL signal is amplified. Here K^{LIA} is the transfer function of the LIA, which can be treated as a constant over the frequency range considered. After inverse Fourier transform, a PL spectrum is obtained as:

$$B_{\mathrm{ss}}^{x}(\tilde{\nu}) = \frac{v_{\mathrm{ref}} K^{\mathrm{LIA}}}{2} B_{\mathrm{PL}}(\tilde{\nu})\cos(\theta_{\mathrm{PL}} - \theta_{\mathrm{ref}}) \quad . \tag{5}$$

Semiconductor samples were tested by this modulation method and compared with the conventional method at a same temperature. The typical results are shown in Fig. 2(b). The PL spectrum indicated by ① is from a mid-infrared HgCdTe sample at 77 K, the solid line is the FTIR-PL spectrum, the dotted line is the ssFTIR-MPL spectrum, which is no longer interfered by the strong suppression of environmental thermal background radiation that was suffered by the conventional FTIR-PL method, and shows clearly distinguishable PL spectral characteristics of the

sample. The background suppression is better than 2500∶1 in the strong environmental background radiation band near 10 μm. The PL spectrum indicated by ③ is from an InGaP/AlGaInP QW sample at room temperature, the solid line is an FTIR-PL spectrum, while the dotted line is the ssFTIR-MPL spectrum. The interference caused by the spectral line of the internal He-Ne laser (632.8 nm, about 1.96 eV) in the spectrometer is suppressed, and the interference suppression ability is better than 1750∶1. Both cases show that the ssFTIR-MPL spectroscopic method can completely eliminate the laser interference inside the system and the thermal background from the environment[25].

It is worth to mention that in 2012 Ullrich and Brown reported the new development of the csFTIR-DMPL spectroscopic technique[16]. However, the fundamental difference between the csFTIR-DMPL and the ssFTIR-MPL still lies in the scanning of the interferometer moving-mirror, and in the former the Fourier frequency $f_{\tilde{\nu}}^{\mathrm{cs}}$ is still not zero, which does not change the limitations of the method first proposed by Fuchs et al[14] and Reisinger et al[15]. By simple estimation, the SNR of the ssFTIR-MPL spectrum is more than 15 times higher than that of csFTIR-DMPL spectrum in terms of nominally identical samples and comparable measurement. Zhang et al[17] compared the csFTIR-DMPL and the ssFTIR-MPL methods, and proved that the latter can effectively eliminate thermal background and is a wise choice for high SNR measurement of weak PL signals.

The ssFTIR-MPL spectroscopic method has been replicated by many research groups, e.g., in Germany, Russia, the United States, Poland, Ukraine, and Israel, and has played an active role in the research of narrow-gap semiconductor materials and devices. Hempel et al[31] used ssFTIR-MPL spectroscopic method in the wavelength range of 0.8−8.0 μm for suppressing the overall thermal background so as to record and analyze the infrared emission of a 980 nm single-mode high-power diode laser, thereby ensured the MWIR emission observed was fully from the laser, and determined the distinct shortwave infrared emission band with a maximum of 1.3 μm originating from defect states in the device waveguide. Morozov et al[32] confirmed that the ssFTIR-MPL method can reduce the spurious signal of room-temperature background radiation by more than two orders of magnitude, and observed the interband PL transition of HgCdTe in the 6−26 μm band and 18−200 K temperature range, which proved radiative transition to be the main mechanism of carrier recombination at high excitation level. Rumyantsev et al[33,34] used ssFTIR-MPL method to study the long-wave infrared stimulated emission and interband emission amplification of optically pumped dielectric waveguide HgCdTe QW heterostructure, and found the continuous wavelength tuning of about 30 μm and the operating wavelength up to 40 μm be achievable by using the technologically achievable extrinsic structure thickness and Reststrahlen effect.

Fadeev et al[35] studied the stimulated emission of thermoelectrically cooled HgTe/CdHgTe QW heterostructure in the wavelength range of 2.8−3.5 μm. It is proved that Peltier cooling is feasible in similar structure lasers, and it is expected to be applied in the spectroscopy of 3-5 μm atmospheric transparency window. Galeeva et al[36] confirmed that the ssFTIR-MPL method can suppress the spurious signals from the environmental thermal radiation and improve the measurement sensitivity, thus contribute to the PL-spectrum measurement in the infrared band. The topological phase transition mixed $(Bi_{1-x}In_x)_2Se_3$ crystal is studied, and it is proved that the topological surface state can be distinguished from other highly conductive surface electronic states by measuring the photoelectric electromagnetic effect using terahertz laser radiation. Motyka et al[37] used ssFTIR-MPL spectroscopic method to study the near 5 μm optical transition of type II QWs. Smołka et al[38] confirmed that ssFTIR-PL spectroscopic method is an effective tool for characterizing narrow-gap semiconductors, and observed PL spectra from ternary InAsSb double heterostructures in the mid-infrared range of 2.5−4.0 μm. Majkowycz et al[39] determined the defect energy levels of $Hg_{1-x}Cd_xTe$(x = 0.17−0.60) materials by ssFTIR-MPL spectroscopic method, and found that the defect energy levels were related to the valence band and did not change significantly with temperature. Arad-Vosk et al[40] deposited thin films of lead sulfide alloyed with thorium and oxygen on GaAs substrates, processed them into photodiode structures, and studied them by ssFTIR-MPL spectroscopy. Jang et al[41] studied the source of high photoresponse in sensitized PbSe films using ssFTIR-MPL spectroscopy to minimize the effect of strong infrared absorption of CO_2, and measured the band gap of PbSe to be 0.29 eV. Chen et al[42,43] used ssFTIR-MPL metho to suppress thermal background radiation noise, studied the bright PL spectra of thin BP film with thickness of 4.5−46 nm in the temperature range of 80−300 K, analyzed the tunable mid-infrared light emission of hexagonal boron nitride (hBN)/BP/hBN heterostructure device, and found that the PL spectrum peak of about 20 layers of BP flakes be continuously tunable from 3.7 μm to 7.7 μm under a displacement field up to 0.48 V/nm.

3.2 Wide-band and condition-controlled ssFTIR-MPL experimental system

Visible-near-infrared PL spectroscopy has been for a long time widely used in the evaluation of semiconductor material’s quality and defects, and for which commercial diffraction spectrometer is a common choice of spectral characterization. The situation is quite different in the infrared band longer than 5 μm, where most narrow-gap semiconductor materials show weak luminescence that is

not suitable for grating spectrometer detection, and hence there was not a commercial PL orientated/optimized spectrometer. On the basis of the validation and application of the ssFTIR-MPL spectroscopic method, we have further developed a universal wide-band multiple condition-controlled ssFTIR-MPL experimental spectroscopic system by solving the problems of band extension, spectral noise reduction, false signal prevention, and controllable excitation/temperature/magnetic-field conditions, which will not only ensure the performance advantages of the ssFTIR-MPL spectroscopic method in a wide infrared band, but also possess the conventional functions in the traditional visible/near-infrared bands, and hence provides a basic guarantee for the efficient analysis of PL spectral characteristics and its regulation of infrared optoelectronic materials.

Figure 3(a) is a schematic of the principle of wide-band condition-controlled ssFTIR-MPL experimental spectroscopic system. The core of the hardware of the system is an FTIR spectrometer with step-scan function. The hardware of the system includes also a controllable pump laser, an optical Dewar with superconducting magnet, a combination of mechanical chopper and LIA, an electronic controller. Magnetic field- and temperature-dependent PL spectra can be measured, also under different excitation energy/power by the combination of selective wavelength (such as 459 nm, 488 nm, 514.5 nm, etc.)/power laser.

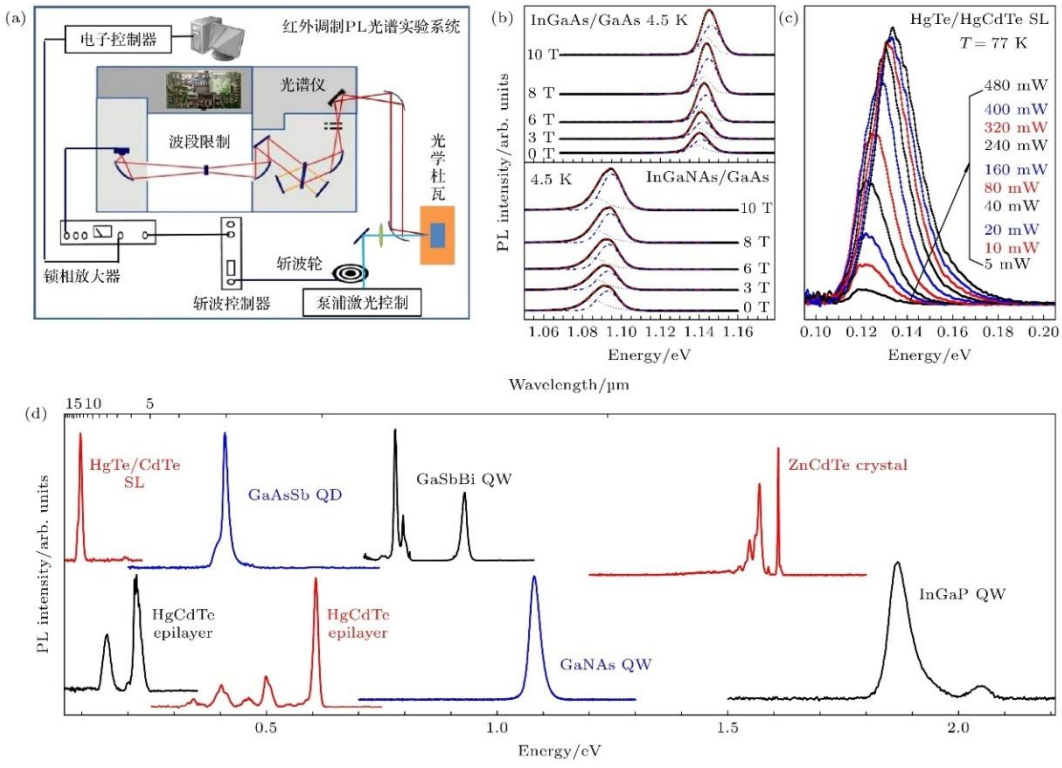

Figure 3. (a) Main components of a wide-band condition-cotrolled ssFTIR-MPL experimental spectroscopic system; (b) low-temperature magneto-PL spectra of InGa(N)As/GaAs QW; (c) excitation power-dependent PL spectra of HgTe/HgCdTe SL at 77 K; (d) PL spectra of different semiconductors in a wide spectral range of 0.56–20 μm.

Figure 3(b) shows typical magnetic field-dependent PL spectra of InGaAs/GaAs and InGaNAs/GaAs QWs at 4.5 K. The PL spectra are significantly blue-shifted with the increase of magnetic field. In Fig. 3(c), typical PL spectra are shown from HgTe/HgCdTe SL at 77 K, of which the PL peak is blue-shifted, the peak width is broadened, and the intensity is increased under the pumping laser power of 5–480 mW. With the equipment of multiple detectors/beam splitters (and appropriate optical windows), the functionality of the system will cover a wide band of 0.56–20 μm. As illustrated in Fig. 3(d), the spectra from either InGaP/AlGaInP QW in the visible band, or GaNAs/GaAs and GaSbBi/GaAs QWs in the near-infrared band, or HgCdTe epitaxial film in the medium-wave infrared, or even HgTe/HgCdTe SL in long-wave infrared, all manifest such high SNR that enough for ensuring quantitative line-fitting analysis.

In the visible-mid-infrared spectral range (of wavelength about 0.6–4.0 μm) where traditional photoluminescence (PL) spectroscopic method is applicable, the above wide-band condition-controlled ssFTIR-MPL experimental spectroscopic system offers advantages of high SNR and stable control conditions, which ensures the acquisition of series temperature-, excitation- and magnetic field-dependent PL spectra, and facilitates research on semiconductor spectral physics.

Temperature-dependent PL studies on $Ga_xIn_{1-x}P/(Al_{0:66}Ga_{0:34})_yIn_{1-y}P$ QWs with CuPt-type long-range ordering reveal the effects of compressive strain and substrate misorientation on the long-range ordering that compressive strain competes significantly with the 6 ° deviation from the $[111]_A$ orientation. Compressive strain not only influences the distribution of different long-range ordered domains in the *x*-*y* plane of the QWs but also introduces fluctuations in long-range ordering along the *z*-direction, leading to PL peak splitting [44].

Temperature- and excitation power-dependent PL studies uncovered anomalous effects of Auger recombination in InGaAs/InAlAs QWs. At low temperatures, an abnormal enhancement of Auger recombination was observed, along with a distinct transition from Auger recombination to Shockley-Read-Hall recombination as temperature increased. These findings suggest that excitation power-dependent PL measurements can effectively assess localized detrimental effects, thereby serves as a convenient evaluation procedure for alloy QWs [45].

Excitation-, temperature-, and magnetic field-dependent PL experiments were employed to investigate the impact of post-growth rapid thermal annealing on the interfaces of InGa(N)As/GaAs QWs. The PL spectra could be reconstructed by two PL-components assumption. Annealing at 750 ℃ reduced the linewidths of the both PL components and decreased their energy separation. The annealing process improved intralayer quality, enhanced In-Ga interdiffusion at the interfaces, and

reduced interface fluctuations. This demonstrates that PL spectral analysis under multiple controllable conditions is effective for probing the interface evolution in QW structures[46].

In an adjustable magnetic fields and at low-temperature, PL measurements were conducted on GaSb/AlGaSb and dilute-bismuth GaSbBi/AlGaSb QWs. Dual-peak PL characteristics and abnormal blueshift were resolved in the dilute Bi sample. The two PL features of the dual-peak was indicated originating from interband transitions, which result from the combined effects of large lateral-scale island-like structures at the interfaces and Al/Ga interdiffusion induced by Bi incorporation. The interdiffusion introduces a contraction of approximately one monolayer in the effective QW thickness, which is similar to the height of the interface islands. The joint effect of these factors is the formation of the unusual shallow terrace-like interface structure between GaSbBi and AlGaSb. The study estimated the isoelectronic Bi content and exciton reduced effective mass in the GaSbBi sample, proposed a bandgap bowing coefficient of approximately 21 meV/%Bi. Additionally, a method was developed to effectively determine the Bi content and the depth of the shallow terraces at the interface in dilute- bismuth QW structures[47].

Low temperature and temperature-dependent PL measurements were conducted on high tensile-strain Ge nanostructures embedded in GaSb matrix. Typical PL quenching of the tensile-strain Ge and GaSb related transitions was observed in the samples with Ge deposition thinner than the critical thickness. In the samples with Ge deposition exceeding the critical thickness, on the other hand, negative PL quenching was observed for GaSb interband transitions. The direct bandgap transition related PL characteristics were distinguished, and the influence of Ge deposition thickness and the thermal quenching mechanism of electron injection from the tensile strain Ge layer to the GaSb matrix were elucidated[48].

In an excitation power- and magnetic field-dependent PL study of the effect of Bi doping on the band tail states of $GaAs_{1-x}Bi_x$ at low temperature, it was found that (i) the broad PL peak contains three PL features and monotonically blue shifts with increasing excitation power; (ii) the PL characteristics are independent of the free exciton recombination with a single Bi content, and the tail filling is the reason for the blueshift of PL peak; (iii) the bandtail density of states increases with the increase of Bi doping level and affects the determination of Bi induced bandgap reduction. The results indicate that the combined analysis of excitation- and magnetic field-dependent PL spectra can effectively detect bandtail states in semiconductors[49].

Temperature-dependent PL spectroscopy was used to study electron-hole recombination and anomalous negative thermal quenching effects below the band gap of $InP_{1-x}Bi_x$. Four PL features

were resolved by spectral line fitting, among which the integration intensities of two high-energy PL features decreased monotonically with the increase of temperature, while the integral intensities of the two low-energy PL features decreased when they were below 180 K, but increased abnormally above 180 K. Within the framework of a phenomenological model, the residual electrons of the PL transition final state are transformed into a non-radiative state through thermal jumping, which generates holes in the final state, and significantly enhances the radiative recombination[50].

Temperature-dependent PL spectroscopic studies of molecular beam epitaxial (MBE) InAsBi films on GaAs substrates showed that the PL peak got blueshifted and broadened with the increase of the Bi/As flux ratio, in clear contrast to the common electron incorporation of Bi or surfactant effects. Based on the linear analysis and the splitting of the PL peak in the magnetic field, the anomaly can be attributed to the Bi flux-induced enhancement of electron concentration. As the Bi/As flux ratio increases from 0 to 1×10^{-3}, the electron concentration in the InAs film increases by about 5 times, indicating that the carrier redistribution in the InAs film is enhanced, while the carrier-phonon Fröhlich scattering is weakened [51].

In the middle infrared band where the traditional method is ineffective and the performance of the csFTIR-DMPL is limited, the fast, stable and high SNR ssFTIR-MPL experimental spectroscopic system ensures the need for quantitative analysis.

In the 1.7-5.4 μm band, temperature- and magnetic field-dependent infrared PL spectra were acquired from p-type $Hg_{1-x}Mn_xTe$ single crystals ($0.20 \leq x \leq 0.26$) in the reflected and transmitted geometry, the evolution of PL spectral characteristics was observed and the zero-field spin splitting of the magnetic polaron bound by the acceptor was determined, and direct evidence of local spontaneous magnetization was obtained[52]. Furthermore, power-, polarization-, and temperature-dependent PL spectra showed giant Zeeman splitting and polarization of PL spectra, and revealed the physical mechanism of photomagnetization, indicating the ssFTIR-MPL method with higher sensitivity and SNR a convenient experimental analysis method to elucidate the photomagnetization effect of semimagnetic semiconductors [53].

Infrared PL spectra of vertical arranged InAs nanowires were recorded successfully by the ssFTIR-MPL experimental spectroscopic system in a wavelength range of 2–5 μm and a wide temperature range of up to 290 K, of which the main PL feature was determined mainly from the type-II optical transition at the interface between zinc-blend and wurtzite InAs, the low-energy PL feature at low temperature was attributed to the impurity-related transition, and the high-energy PL feature at high temperature was due to the activation of the wurtzite InAs interband transition by

heat-induced electron transfer. The results show that infrared PL spectroscopy in a wide range of temperatures can elucidate the optical properties and bandedge processes of the crystalline interfaces of vertically arranged InAs nanowires[54].

In the mid-to-far infrared band where the csFTIR-DMPL method is severely limited and quantitative analysis is hard to guarantee, SNR ssFTIR-MPL experimental spectroscopic system ensures the requirements for quantitative and series spectral analysis with high sensitivity, high spectral resolution, and high SNR.

Interfacial roughness of InAs/GaSb SL is a key issue affecting the performance of infrared photodetectors. Post-growth rapid thermal annealing effect on the InSb-like interface in InAs/GaSb SL was studied by temperature- and excitation power-dependent ssFTIR-MPL spectroscopy, and the changes of PL peak energy, linewidth and integral intensity with temperature indicate that the PL process is dominated by the electron-phonon interaction near the InSb-like interface and adjacent narrow InAs layer, and the interfacial electron level acts as the first thermal escape channel for mini-band electrons and affects SL high temperature characteristics. Annealing promotes interfacial atomic exchange and changes the thermal escape energy of electrons, and the optimized annealing temperature is crucial to improve the SL performance by post-growth annealing. The results indicate that ssFTIR-MPL spectroscopy can be used as an effective reference standard for material optimization[55]. With magnetic field-dependent ssFTIR-MPL measurements, two types of interfacial roughness were quantitatively resolved from the evolution of the PL linewidth in two InAs/GaSb SLs infrared magneto-PL spectral width with nominally identical period, of which one is long lateral length fluctuation aggravated by lattice mismatch and the other short lateral length fluctuation related to interfacial atomic exchange, and it is proved that benefited with the ssFTIR-MPL method, the magneto-PL spectral linewidth can be used as an effective tool to evaluate the effects of SL micro-fluctuation and interfacial roughness on the electro-optical performance[56].

In temperature- and magnetic field-dependent ssFTIR-MPL studies of GaInSb/InAs/AlSb QWs with typical InSb- and GaAs-like interfaces, it is found that as temperature rises, the PL energy is blue-shifted at slightly below 50 K, but red-shifted and broadened rapidly at higher than 50 K. The mechanism can be correlated with the interfacial roughness-related layer thickness fluctuation equivalent to about 9.5-meV localization energy. The PL intensity decreases monotonically with the increase of the magnetic field, which can be attributed to the electron-hole separation induced by interfacial roughness in type-II QWs. The magnetic field dependence of the PL energies in both localized and non-localized states follows typical exciton diamagnetic shift, and the exciton binding

energy, reduced effective mass, and averaged range of wave function derived by this method are not sensitive to the interface type, and the interface type has no significant effect on the localization of the carriers and in-plane exciton behaviors[57].

In a wavelength range of 3-18 μm, as-grown and p-type annealed As-doped HgCdTe epitaxial films were studied by temperature-dependent ssFTIR-MPL method, and it was found that the transition between the conduction band and the valence band could only be detected at 77 K, enhanced to dominate the PL line above about 200 K, and was mainly related to impurities as temperatures lower than 100 K. The V_{Hg}, As_{Te} acceptor levels were determined to be located at 12 and 20 meV above the valence band, and As_{Hg}, and Te_{Hg} donor levels 17 and 26 meV below the conduction band, respectively. The results show that the ssFTIR-MPL spectroscopic method can be used as a convenient and reliable way to characterize narrow-gap HgCdTe impurities only when PL spectra can be recorded with high SNR in a wide temperature range up to near room temperature[58]. Temperature- and excitation power-dependent ssFTIR-MPL measurements of HgTe/$Hg_{0.05}Cd_{0.95}Te$ SLs showed that the linewidth of the whole PL peak at 11 K was only about 7 meV, though on the basis of the PL lineshape evolution with temperature, three PL components of low, medium and high energies could be resolved, and different changes of energy, linewidth and intensity were found. The high-energy component originates in electron to heavy hole transition, the low-energy component correlates to localized states, and the high-energy component is due to interfacial inhomogeneity chemical mixing and Brillouin zone boundary effect. The low- and high-energy correlated effects dominate the PL intensities of the SL at well below and above 77 K, respectively[59].

In a wide wavelength range of 1.3-17.7 μm, ssFTIR-MPL measurements of the subband transitions of InGaAs/InAlAs quantum cascade detector structure were realized with high SNR by configuring tilted and parallel excitation geometries, and the temperature evolution of the PL spectra show that the transition caused by longitudinal optical phonon-assisted scattering plays an important role in the inter-subband transition, indicating the wideband ssFTIR-MPL spectroscopy possessing great potential in the characterization and performance diagnosis of quantum cascade detectors[60].

The advanced reliability of the wideband ssFTIR-MPL experimental spectroscopic system provides also a convenient way for cooperative research and testing support, and plays an effective role. Zha *et al* employed the ssFTIR-MPL experimental spectroscopic system to characterize the n-on-p HgCdTe photodiodes realized by ion etching, found that the PL peak in the n-type transition region shifted to higher energy, and its value was about 40 meV more than that in the p-type region, and considered the blueshift be due to the Burstein-Moss effect associated with the high electron

concentration in the type transition region[61]. Zhang *et al* used the wideband ssFTIR-MPL experimental spectroscopic system together with infrared photoreflectance method for analyzing the optical transitions of epitaxial PbTe films epitaxially grown on BaF_2 (111) substrates, and found that the intrinsic defect energy levels in the electronic structure have resonant properties[62]. Deng *et al* investigated by temperature- and excitation power-dependent PL spectroscopy the effect of p-type Be-doping on the optical properties of the GaSb layer molecular-beam epitaxially grown on GaAs substrates[63]. Zhuang *et al* successfully fabricated optically efficient InAsSb nanowires, obtained the room-temperature PL emission of InAs nanowires, and extended with success the PL emission wavelength of InAsSb nanowires to 5.1 μm, enabling operation in the mid-wave infrared band of silicon-based optoelectronic devices[64].

Huang *et al* found that when the growth temperature decreased from 380 ℃ to 340 ℃, the PL peak of the InAs/GaSb SL structure shifted from 5.8 μm to 4.0 μm at 77 K, and considered increasing the thickness of the GaSb layer in the structure as an effective method to achieve a detection wavelength of 2-3 μm[65]. Xing *et al* investigated the effects of the InAs/GaInSb and InAs/AlSb interfaces on the optical properties of AlSb/GaInSb/InAs QWs using excitation power- and temperature-dependent ssFTIR-MPL spectroscopic method, analyzed the localized states and activation energies, and discussed possible mechanisms of thermal quenching and non-radiative recombination[66]. Pan *et al* studied the PL performance of InGaAs/GaAsBi/InGaAs QWs molecular-beam epitaxially grown on GaAs substrates by using excitation power- and temperature-dependent PL spectroscopic method, and found that thermal excitation process resulted in band bending relaxation, and the type-II PL transition was rapidly quenched and redshifted with increasing temperature[67]. Chen *et al* grew by MBE Ge QD structures of different sizes with high tensile strain on InP substrates, achieved a direct bandgap transition PL spectrum with a peak energy of 0.796 eV, and confirmed the nature of direct bandgap PL transition by etching depth-, temperature-, and excitation power-dependent PL analyses, which provides evidence for the future photonics application of high-tensile strain semiconductor nanostructures[68]. Xu *et al* employed the ssFTIR-MPL spectroscopic method for the study of optimization and control of InSb interface properties during the molecular-beam epitaxial growth SL structures[69].

3.3 High-throughput scanning imaging ssFTIR-MPL experimental system

The pixel-level response inhomogeneity of IRFPA photodetectors limits the performance of infrared imaging systems. Semiconductor materials and processes determine the uniformity of the

detector response, and accurate detection and quantitative evaluation are the keys to determine the source of inhomogeneity and to improve the imaging performance of IRFPA detectors. Visible and near-infrared PL spectral imaging is theoretically non-destructive, fast and easy, and is a very effective characterization method for evaluating the spatial uniformity of semiconductor materials. Near-field PL spectral imaging with grating as a dispersive element can provide sub-micron spatial resolution, but it is not suitable for the long-wavelength infrared bands beyond about 4 μm. In order to overcome this limitation, Furstenberg et al reported in 2004 preliminary results of PL scanning imaging experiments in mid-infrared[70]. Using the csFTIRDMPL spectroscopic method together with a confocal microscope and scanning stage, they achieved the scanning imaging of 3-4 μm infrared radiation from an epitaxial $Hg_{0.7}Cd_{0.3}Te$ layer with a spatial resolution of about 22 μm and a single-point PL spectral SNR of not better than 3. In 2006, Furstenberg et al further reported a csFTIRDMPL system that can measure weak infrared PL spectra from with diffraction-limited resolution and perform spatial imaging[8], and obtained PL spectra (of center wavelength about 3.5 μm at room temperature a) from a typical HgCdTe epitaxial film with an effective spatial resolution of 10-15 μm and a spectral resolution of 16 cm^{-1}. The SNR was however, only about 2.In 2015, Dyksik et al reported the results of the ssFTIR-MPL spectroscopic method for the measurement of mid-infrared spatially resolved and scanning imaging PL spectroscopy of 2-inch GaSb- and InAs-substrate type-II InAs/GaInSb QW structure wafers[71]. The spatial resolution is defined by the pumping beam diameter of about 700 μm on the sample surface, a PL spectrum with central wavelength of about 6.4 μm was achievable in a time period of 5 min with a SNR of about 10, and that collecting about 360 PL spectra per wafer costed a total measurement time of 30 h. In 2019, Pepper et al collected infrared PL spectra at different spatial positions in a 10×10 grid with a step size of 0.381 mm and a total scanning area of 3.81 mm × 3.81 mm on the surface of an InAsSb sample using FTIR spectrometer in the step-scan mode, 50 kHz frequency modulated 643 nm laser excitation, and signal readout by LIA, and observed the spatial variation of 14-meV PL-peak blue shifting and the localization effects of minority carrier lifetime shortening[72]. In 2021, Kwan et al employed infrared PL spectroscopy and high-resolution X-ray diffraction to compare the optical and structural properties of MBE grown InAs/GaSb SLs on different substrates of GaAs and GaSb. A 785 nm laser was modulated at 20 kHz and the background signal was subtracted by a LIA, the PL signal was collected by an FTIR spectrometer equipped with a liquid nitrogen-cooled HgCdTe detector, and spatial correlation of PL spectra was measued at five different locations on the sample surface to confirm the inhomogeneity caused by increase in SL defects[73].

By solving technical problems of isometric strong focusing, long-term stable control of excitation

light direction and intensity, coaxial visible excitation and infrared detection, and long-term constant temperature control of samples, we have further improved the experimental sensitivity, shortened the experimental time, realized the ability of high-throughput scanning imaging infrared modulated PL spectroscopy, and achieved an order of magnitude improvement compared with the previously reported results in key performance such as spectral SNR and measurement efficiency[74].

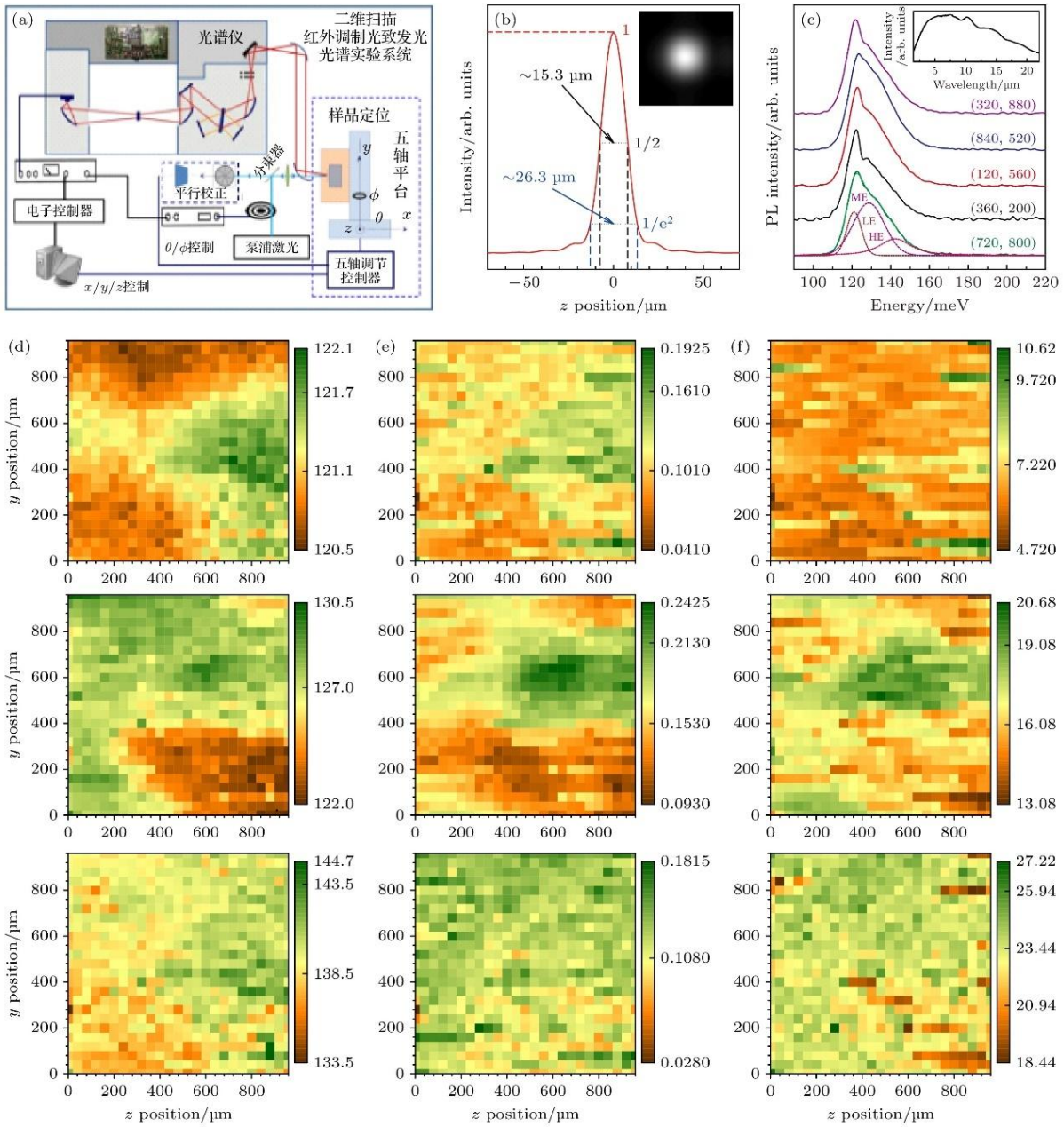

Figure 4. (a) Main components of scanning imaging ssFTIR-MPL experimental spectroscopic system; (b) spatial profile of 532 nm pumping light intensity at the common focus of the lens and parabolic mirror, 1/2 and 1/e^2 peak intensities correspond to spot diameters of 15.3 and 26.3 μm, respectively, insert for spot picture[74]; (c) typical PL spectra of HgTe/HgCdTe superlattice at 5 different (y, z) coordinate positions, that at (720, 800) fitted with LE, ME and HE PL features, inset for system response with inner globar source[74]; (d)–(f) energy, intensity, and FWHM images of the LE, ME, and HE PL features of 25×25-pixel PL spectra on a 960 μm×960 μm surface part of HgTe/HgCdTe superlattice[74].

Figure 4(a) illustrates the principle of the scanning imaging ssFTIR-MPL experimental spectroscopic system. The laser output is modulated by a chopper (the modulation frequency is also used as the reference to the LIA) after passing through a long-term stabilization unit, and is fed into the coaxial focusing optical path through a beam splitter, and finally forms a spot with a diameter of about 30 μm on the sample surface. The sample is placed in a cryogenic optical dewar to achieve a long-term stable control of different temperatures; The optical dewar is set on a five-dimensional mechanical platform to adjust the step position of the sample relative to the laser spot in the y, z direction of 20-30 μm. The laser incident on the sample surface is partially reflected and enters the laser positioning unit of the parallel correction system via the beam splitter, and the two-dimensional angle control of the platform is determined to ensure that the spatial position of the intersection of the light spot and the sample surface is constant during the scanning imaging process. The infrared PL signal from the sample is fed into the FTIR spectrometer through the off-axis parabolic mirror system, and irradiated to the detector after passing through the interferometer and band limiter. The detector output is transformed into the final PL spectrum after LIA demodulation. Commercial components such as FTIR spectrometer ensure the possibility of infrared modulation PL spectroscopy method and system implementation from the hardware point of view, and the integration of components and systems such as self-made optical path determines the actual two-dimensional spatial resolution and the test effectiveness of scanning imaging infrared PL spectroscopy. Different combinations of beam splitters, detectors and band limiters can be used to achieve a wide-band of 2-20 μm scanning imaging ssFTIR-MPL measurement. The spatial resolution is mainly limited by the minimum size of the achievable excitation spot. Figure 4(b) shows the measured results of the excitation spot diameter, according to the different definitions of baseline half-height and $1/e^2$, the minimum spot diameter is 15.3 and 26.3 μm, respectively, that is, the spatial resolution of the scanning imaging ssFTIR-MPL experimental spectroscopic system is better than 16 μm according to the conventional definition of full-width at half-maximum (FWHM) [74].

Figure 4(c) shows the typical infrared PL spectra of five different (*y*, *z*) coordinate positions in the process of scanning imaging of HgTe/HgCdTe SL at 77 K, and the inset shows the response wavelength range of the experimental system using the internal Globar source. The spectral resolution is 12 cm^{-1}, the measurement time of a PL spectrum is 30 s and the SNR is better than 30 for the center wavelength of 10 μm, which may ensure reliable spectral line-fitting to resolve energetically very close different PL processes[72]. Three-feature fitting of the PL spectrum at (720, 800) is labeled with low energy (LE), medium energy (ME), and high energy (HE), which originate in the localized state related, inter-subband, interfacial mixing and/or Brillouin zone boundary effect

related transitions, respectively[59].

Figures 4(d)-(f) shows the LE, ME, and HE PL-feature images of energy, intensity, and FWHM from the 25×25 pixel PL spectra on a 960×960 μm^2 surface element of HgTe/HgCdTe SL sample. Obviously, the in-plane energy distribution of the three PL components is non-uniform, and the region of high LE energy coincides with the region of high ME energy in a certain degree, which means that there is intrinsic relationship between the localized states and the inter-subband transition in the same region. The intensity image reveals the radiative recombination and the number of photogenerated carriers, while the linewidth image reflects the influences of phonon scattering and microstructure on the electronic energy levels[74].

Compared with the csFTIR-DMPL spectroscopic method used by Furstenberg et al[70], the inherent advantages of the ssFTIR-MPL spectroscopic method ensure a wider spectral range, higher spectral resolution and SNR, and can warrant line-fitting of infrared PL spectra to quantitatively analyze the in-plane distribution of PL energy, intensity and FWHM. Compared with Dyksik et al[71] who also used ssFTIR-MPL spectroscopic method[25], realized mid-infrared (with a central wavelength of about 6.4 μm) spatial resolution and scanning imaging PL with a laser pump spot of about 700 μm, and measured a PL spectrum in 5-min with a SNR of about 10, the comparative advantage of our system is the integrated design of the scanning imaging experimental system, the home-made key optical path and the system integration optimization. The results indicate that scanning imaging ssFTIR-MPL experimental spectroscopic system can provide an effective way to study the microscopic mechanism and in-plane distribution of the optoelectronic properties of narrow-gap semiconductor IRFPA materials.

It is worthy to note that for the above-mentioned long-wave infrared measurement, if the requirements for the spectral SNR are appropriately reduced to, e.g. 15, then the single-spectrum measurement time can be shortened to 8 s, and the PL measurement of up to 50×50 pixels can be completed in 8 h. For mid-wave infrared, a SNR of not less than 25 can be achieved with the same measurement time[74], reaching a practical “high-throughput” measurement level.

The scanning imaging ssFTIR-MPL experimental spectroscopic system has ensured preliminary applications and made significant research progress [75–77]. The pixel uniformity of InAs/GaSb SL IRFPA is affected by the in-plane uniformity of the SL material. Although the layer thickness is controllable at a single-monolayer level, the photoelectric uniformity of InAs/GaSb SL is still a challenge due to lattice mismatch and interface roughness. To this end, we have carried out a scanning imaging ssFTIR-MPL measurement with a spatial resolution of typical IRFPA pixel sizes[75].

In the 6-14 μm band, 16×16-pixel PL spectra were obtained from InAs/GaSb SL at 77 K with 30-μm spatial resolution and 12 cm^{-1} spectral resolution, and the spatial distribution of peak energy, linewidth and integral intensity was analyzed. It was found that the in-plane uniformity of the effective band gap was very high, the peak energy deviation of PL peak was only about 0.5%, and the relative deviation of PL linewidth was also very low, but the relative deviation of radiation recombination was obviously high at 4.7%. The in-plane distribution of the effective carrier lifetime and Shockley-Read-Hall defect concentration was evaluated by using the excitation power-dependent model of PL integral intensity, which suggested that the inhomogeneity of the photoelectric response may limit the performance of the IRFPA photodetector fabricated. The results indicate that the scanning imaging ssFTIR-MPL experimental spectroscopic system can be used as an effective new way to analyze the uniformity of IRFPA materials in the infrared, especially in the long-wave infrared.

$Hg_{1-x}Cd_xTe$ as the preferred material for high-performance IRFPA, arsenic (As) doping is a favorable method to achieve p-type conductivity, but at the same time, it has also "amphoteric" behavior, and tends to act as n-type dopant during MBE growth. For IRFPA applications, the spatial uniformity of the banded structure is particularly important. In the past, only csFTIR-DMPL method-based scanning imaging report was seen, and only the near-banded edge PL spectral profile was obtained, impurity-related transitions remained unresolved[70]. To this end, we carried out a scanning imaging ssFTIR-MPL study on MBE-grown As-doped HgCdTe[76], and obtained 21×10 pixel PL spectra in a wavelength range of 3-6.5 μm with spatial resolution of 30 μm and spectral resolution of 8 cm^{-1}. The spatial distribution of PL peak energy, linewidth, and integral intensity was analyzed. It was found that although the in-plane PL peak energy was highly uniform and the spatial variation was within 1 meV, the spectral lineshape clearly showed multi-near bandedge transition characteristics, and the difference in spectral lineshape is significant among the pixels. The integral PL intensity fluctuated significantly, and the maximum relative fluctuation was as high as 35%. The results show that it was not reasonable and reliable to judge the bandgap uniformity simply by the PL peak energy[70]. The PL transitions related to band gaps, V_{Hg}, As_{Hg}, and As_{Hg}–V_{Hg} pairs were resolved by the evolution of temperature-dependent PL spectra, and the spatial inhomogeneity of Cd components and the distribution of relative concentrations of V_{Hg}, As_{Hg}, As_{Hg}–V_{Hg} were hence estimated. The results show that As atoms directly replace Hg atoms in the complete lattice or occupy the existing V_{Hg} to form As_{Hg}, which leads to spatial fluctuations in conductivity and may damage the performance of IRFPA. The inter-band transition characteristics reflecting the distribution of Cd components show maximum energy inhomogeneity, and the fluctuation range is

about 3.7 meV. This is different from that solely using the PL peak energy as the criterion for in-plane uniformity of the band gap, highlights the importance of distinguishing complex transitions and identifying inter-band transitions for evaluating the in-plane distribution of As-doped HgCdTe, and indicates the scanning imaging ssFTIR-MPL experimental spectroscopic system an effective evaluation tool[76].

3.4 Spatially resolved ssFTIR-μPL experimental system

With the continuous reduction of pixel size (as small as 3-5 μm) and expansion of the scale of the IRFPA devices, μm-scale uniformity constitutes the bottleneck for the further improvement of IRFPA performance, and it is extremely important and urgent to develop effective experimental methods for uniformity evaluation. Quantum manipulation- and nanostructure-based infrared materials have attracted great attention in recent years, and the relevant fundamental physics of semiconductor materials and the application of single-photon devices have been developing in the direction of quantum/nanowires, QDs, and single-point defects (about 10 μm or even less in HgCdTe), which also put forward high requirements for the spatial resolution and applicable bands of infrared PL spectroscopy.

The new challenge of infrared modulated micro-PL (IRM-μPL) spectroscopy is that in order to ensure that the sample is not ablated and the band-edge transition is detectable, the excitation power density must be controlled at a reasonably low level, which requires that the excitation light power be reduced by 1-2 orders of magnitude relative to the scanning imaging described in Section 3.3 in response to the decrease of the excitation spot size. The sharp decrease in the number of pump photons will inevitably further test the detection ability. In fact, early in 2006, Furstenberg *et al* [8] tried a μPL measurement with a center wavelength of about 3.5 μm based on the csFTIR-DMPL spectroscopic method, the obtained spectral SNR is however only about 2, and since then no further application progress has been reported.

Based on the wide-band ssFTIR-MPL spectroscopic method, we solved the technical problems of coaxial visible excitation and infrared detection by a reflective objectives, and established a 2 μm-level spatially resolved IRM-μPL spectroscopic method and experimental system[78].

Figure 5(a) illustrates the principle of the IRM-μPL experimental system. In order to achieve a spatial resolution of better than 3 μm, the magnification of the reflective objective lens was selected, and a laser beam collimation expander was used together to form an excitation spot with a diameter

of about 2 μm on the sample surface. A dichroic filter was used to realize the real-time monitoring of the sample and the laser spot. The sample is set in a cryogenic optical dewar to achieve long-term stable control of temperatures. The optical dewar is placed on a five-dimensional μm-level adjustment mechanical platform [the coordinates are defined as in Fig. 4(a)] to realize the step position adjustment of the sample relative to the laser spot in the y-z plane with positioning accuracy better than 0.5 μm. The PL signal is collimated and output to the front-end beam of the splitter through the same reflective objective, and is then reflected to the off-axis parabolic mirror near the inlet of the FTIR spectrometer, fed into the FTIR spectrometer, and focused on the detector after passing through the interferometer and band limiter. The detector output is preamplified by high-speed low-noise pre-amplification, sent to a LIA for demodulation, and converted into the final PL spectrum by relevant electronic control system. Different combinations of beam splitters, detectors and band limiters can be used to achieve PL measurement in a wide range of 2-20 μm.

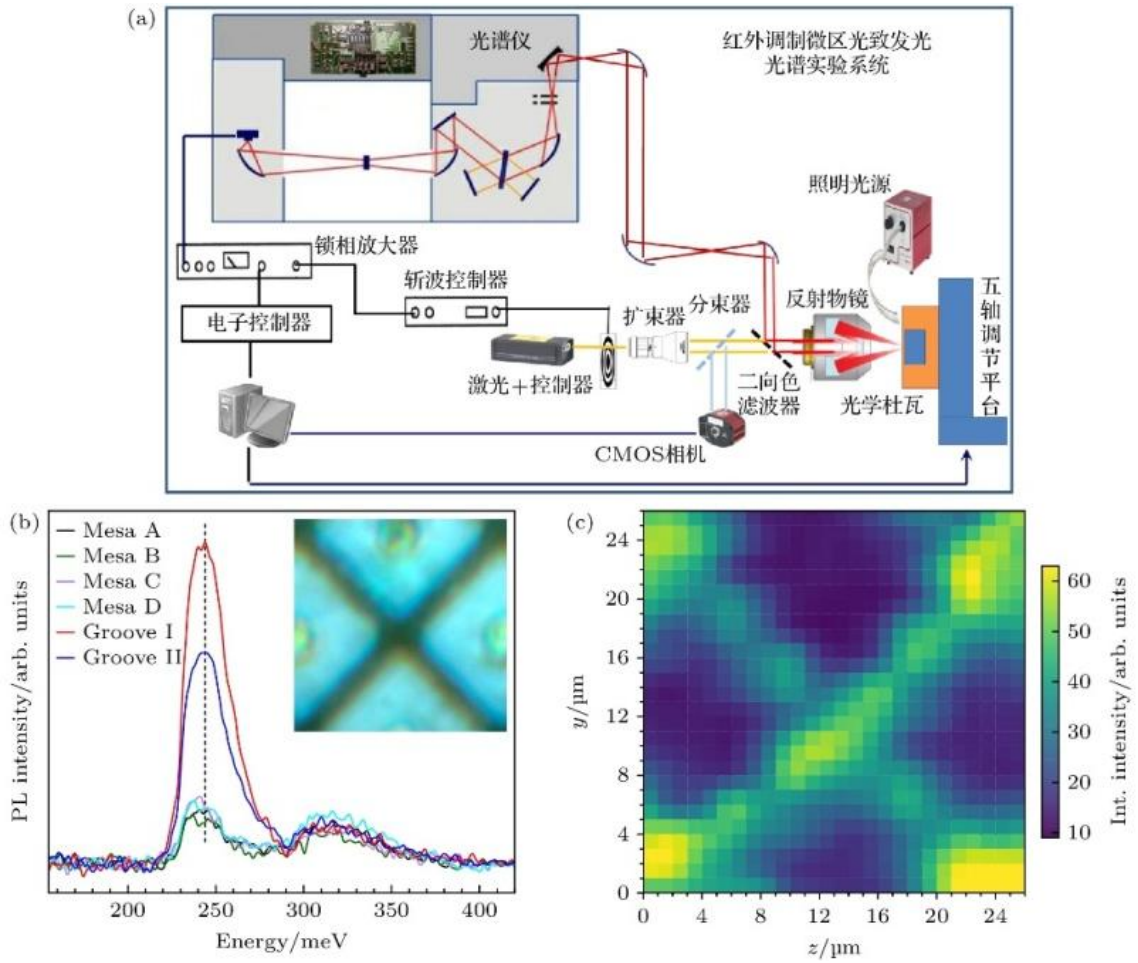

Figure 5. (a) Main components of the IRM-μPL spectroscopic system; (b) representative μPL spectra recorded at different mesas and grooves, low- and high-energy PL components from infrared absorption layer and electron barrier layer of InAs/GaSb superlattice, vertical dashes for peak energy variation of the low-energy PL component, inset for optical morphology of the μPL mapped area[78]; (c) spatial distribution of integral intensity of the low-energy PL component in the measured area of InAs/GaSb superlattice[78].

In order to evaluate the actual spatial resolution of the IRM-μPL spectroscopic system, an InAs/GaSb SL sample containing etch cells of typical width of 2-3 μm was selected and cooled to 77 K in a continuous-flow liquid nitrogen optical dewar. The spectral resolution was set to 16 cm^{-1}, and a time-duration of about 35 s was needed for measuring a single PL spectrum. The complete measurement took about 2 h for spatially resolved imaging with a step size of 2 μm and a sample surface of 14×14 pixels.

Figure 5(b) shows typical infrared μPL spectra with laser focusing on different mesas and grooves of the InAs/GaSb SL, the inset shows the optical morphology of the sample surface in the μPL test captured by a CMOS camera, two grooves in different directions are labeled as Grooves I and II, and four successive mesas are labeled Mesa A, B, C and D. It can be seen that the PL spectral lineshape includes a low-energy spectral component around 220-290 meV (center wavelength of about 5.2 μm, spectral SNR up to 20) and a high-energy spectral component of 290-370 meV, and are originated from the infrared absorber layer and the electron barrier layer, respectively. The vertical dashes show the change of the low-energy PL peak energy. The obvious change of the low-energy PL component intensity indicates a significant difference between the mesa and the groove. Figure 5(c) is an image of the in-plane distribution of the integral intensities of the low-energy PL component[78]. Although the width of the etch cell is only 2-3 μm, it can still be clearly identified, which proves the IRM-μPL a spatial resolution of 2-3 μm with a spectral SNR being 10 times higher than that of the csFTIR-DMPL method[8]. For comparison, Table 1 lists the reported key parameters of, e.g., the spatial resolution of infrared scanning imaging PL spectra, which can intuitively judge the advantages of the method and the measurement results.

Table 1. Comparison of spatial resolution and other parameters of scanning imaging infrared PL spectroscopy by different research groups.

Literature	Method	Central wavelength (μm)	Spatial resolution (μm)	Spectral resolution (cm^{-1})	Time per spectrum (s)	Signal to noise	Imaging scales
[8]	csFTIR-DMPL[14,15]	3-4	10-15	16	10	≤ 2	48×48
[71]	ssFTIR-MPL[25]	6.4	700	na	300	10	360
[72]	na	10	na	na	na	10	5
[73]	ssFTIR-MPL[25]	4.4	381	na	na	50	10×10
[74]	ssFTIR-MPL[25]	10	26	12	30	30	25×25
[78]	ssFTIR-MPL[25]	5.2	2-3	16	35	20	14×14

4. Conclusion

The PL signal of infrared semiconductor is usually very weak, and is strongly suppressed by the ambient thermal background radiation, which makes the PL spectral measurement severely plagued for a long time. The sFTIR-MPL spectroscopic method that was based on step-scan FTIR spectrometer and reported in 2006 completely eliminates the thermal background radiation interference, breaks the Fourier frequency constraint of continuous scanning of FTIR interferometer, and solves the problem of low sensitivity and limited applicable range of the csFTIR-DMPL spectroscopic method[25]. The effectiveness of the spectroscopic method has been widely verified, and has been adopted by many research groups and applied to the studies of different materials, effectively promoting the study of electronic bandgaps, impurities/defects, and interfaces of narrow-gap semiconductors such as HgCdTe epitaxial films, HgTe/HgCdTe SLs, and InAs/GaSb SLs. Meanwhilee, it also lays the foundation for the development of wide-band sFTIR-MPL experimental spectroscopic system, high-throughput scanning imaging ssFTIR-MPL experimental spectroscopic system, and spatially resolved IRM-μPL experimental system, so as not only cover effectively the long-wavelength infrared of 20 μm, but also warrant efficiently high-throughput scanning imaging with more than 1000 pixels and spatially resolved IRM-μPL study with 2-μm spatial resolution.

As recent developments, the high-throughput scanning imaging ssFTIR-MPL spectroscopic method reported in 2019 has demonstrated unprecedented functional effectiveness in resolving complex transitions in doped HgCdTe epitaxial films, evaluating the in-plane distribution uniformity of near-band edge transitions, analyzing the in-plane distribution of the effective carrier lifetime and defect concentration of InAs/GaSb SL, and evaluating the inhomogeneity of the photoelectric response[74]. The effectiveness of the spatially resolved IRM-μPL spectroscopic method reported in 2024 for μm-scale spatial resolution and spectral quantitative analysis has also been preliminarily demonstrated and verified[78]. It is expected that both methods will play significant roles in the research areas such as pixel-level and sub-pixel-level uniformity of narrow-gap semiconductor IRFPA materials, single defect states, individual nanowires, and single QDs.

References

[1] Fonoberov V A, Pokatilov E P, Fomin V M, Devreese J T 2004 Phys. Rev. Lett. 92 127402

[2] Wang Q Q, Muller A, Cheng M T, Zhou H J, Bianucci P, Shih C K 2005 Phys. Rev. Lett. 95 187404

[3] Jho Y D, Wang X, Kono J, Reitze D H, Wei X, Belyanin A A, Kocharovsky V V, Kocharovsky Vl V, Solomon G S

2006 Phys. Rev. Lett. 96 237401

[4] Jones R E, Yu K M, Li S X, Walukiewicz W, Ager J W, Haller E E, Lu H, Schaff W J 2006 Phys. Rev. Lett. 96 125505

[5] Shao J 2003 Acta Phys. Sin. 52 1743

[6] Bignazzi A, Grilli E, Radice M, Guzzi M, Castiglioni E 1996 Rev. Sci. Instrum. 67 666

[7] Barbillat J, Barny P L, Divay L, Lallier E, Grisard A, Deun R Van, Fias P 2003 Rev. Sci. Instrum. 74 4954

[8] Furstenberg R, Soares J A, White J O 2006 Rev. Sci. Instrum. 77 073101

[9] Liu M, Wang C, Zhou L Q 2019 Chin. Phys. B 28 037804

[10] Eich D, Schirmacher W, Hanna S, Mahlein K M, Fries P, Figgemeier H 2017 J. Electron. Mater. 46 5448

[11] Yang X L, Arita M, Kako S, Arakawa Y 2011 Appl. Phys. Lett. 99 113106

[12] Deshpande S, Das A, Bhattacharya P 2013 Appl. Phys. Lett. 102 161114

[13] Basnet R, Sun C, Wu H, Nguyen H T, Rougieux F E, Macdonald D 2018 J. Appl. Phys. 124 243101

[14] Fuchs F, Lusson A, Wagner J, Koidl P 1989 Proc. SPIE 1145 323

[15] Reisinger A R, Roberts R N, Chinn S R, Myers II T H 1989 Rev. Sci. Instrum. 60 82

[16] Ullrich B, Brown G J 2012 Rev. Sci. Instrum. 83 016105

[17] Zhang Y G, Gu Y, Wang K, Fang X, Li A Z, Liu K H 2012 Rev. Sci. Instrum. 83 053106

[18] Tomm J W, Herrmann K H, Hoerstel W, Lindstaedt M, Kissel H, Fuchs F 1994 J. Cryst. Growth 138 175

[19] LentzG, Magnea N, Mariette H, Tuffigo H, Feuillet G, Fontenille J, Ligeon E, Saminadayar K 1990 J. Cryst. Growth 101 195

[20] Fuchs F, Schneider H, Koidl P, Schwarz K, Walcher H, Triboulet R 1991 Phys. Rev. Lett. 67 1310

[21] Kasai J, Katayama Y 1995 Rev. Sci. Instrum. 66 3738

[22] Freeman J R, Brewer A, Beere H E, Ritchie D A 2011 J. Appl. Phys. 110 013103

[23] Ikezawa M, Sakuma Y, Zhang L, Sone Y, Mori T, Hamano T, Watanabe M, Sakoda K, Masumoto Y 2012 Appl. Phys. Lett. 100 042106

[24] Nguyen H T, Han Y, Ernst M, Fell A, Franklin E, Macdonald D 2015 Appl. Phys. Lett. 107 022101

[25] Shao J, Lu W, L ü X, Yue F Y, Li Z F, Guo S L, Chu J H 2006 Rev. Sci. Instrum. 77 063104

[26] Shao J, Yue F Y, L ü X, Lu W, Huang W, Li Z F, Guo S L, Chu J H 2006 Appl. Phys. Lett. 89 182121

[27] Shao J, L ü X, Lu W, Yue F Y, Huang W, Li N, Wu J, He L, Chu J H 2007 Appl. Phys. Lett. 90 171101

[28] Shao J, Ma L L, L ü X, Lu W, Wu J, Zha F X, Wei Y F, Li Z F, Guo S L, Yang J R, He L, Chu J H 2008 Appl. Phys. Lett. 93 131914

[29] Shao J, Chen L, L ü X, Lu W, He L, Guo S L, Chu J H 2009 Appl. Phys. Lett. 95 041908

[30] Shao J, Chen L, Lu W, L ü X, Zhu L Q, Guo S L, He L, Chu J H 2010 Appl. Phys. Lett. 96 121915

[31] Hempel M, Tomm J W, Yue F Y, Bettiati M A, Elsaesser T 2014 Laser Photonics Rev. 8 L59

[32] Morozov S V, Rumyantsev V V, Antonov A V, Maremyanin K V, Kudryavtsev K E, Krasilnikova L V, Mikhailov N

N, Dvoretskii S A, Gavrilenko V I 2014 Appl. Phys. Lett. 104 072102

[33] Rumyantsev V V, Dubinov A A, Utochkin V V, Fadeev M A, Aleshkin V Y, Razova A A, Mikhailov N N, Dvoretsky S A, Gavrilenko V I, Morozov S V 2022 Appl. Phys. Lett. 121 182103

[34] Rumyantsev V V, Mazhukina K A, Utochkin V V, Kudryavtsev K E, Dubinov A A, Aleshkin V Y, Razova A A, Kuritsin D I, Fadeev M A, Antonov A V, Mikhailov N N, Dvoretsky S A, Gavrilenko V I, Teppe F, Morozov S V 2024 Appl. Phys. Lett. 124 161111

[35] Fadeev M A, Rumyantsev V V, Kadykov A M, Dubinov A A, Antonov A V, Kudryavtsev K E, Dvoretskii S A, Mikhailov N N, Gavrilenko V I, Morozov S V 2018 Opt. Express 26 12755

[36] Galeeva A V, Egorova S G, Chernichkin V I, Tamm M E, Yashina L V, Rumyantsev V V, Morozov S V, Plank H, Danilov S N, Ryabova L I, Khokhlov D R 2016 Semicond. Sci. Technol. 31 095010

[37] Motyka M, Sek G, Misiewicz J, Bauer A, Dallner M, Hofling S, Forchel A 2009 Appl. Phys. Express 2 126505

[38] Smołka T, Motyka M, Romanov V V, Moiseev K D 2022 Materials 15 1419

[39] Majkowycz K, Murawski K, Kopytko M 2024 Infrared Phy. Technol 137 105126

[40] Arad-Vosk N, Beach R, Ron A, Templeman T, Golan Y, Sarusi G, Sa'ar A 2018 Nanotechnol. 29 115202

[41] Jang M, Litwin P M, Yoo S, McDonnell S J, Dhar N K, Gupta M C 2019 J. Appl. Phys. 126 105701

[42] Chen C, Chen F, Chen X L, et al. 2019 Nano Lett. 19 1488

[43] Chen C, Lu X B, Deng B C, Chen X L, Guo Q S, Li C, Ma C, Yuan S F, Sung E, Watanabe K, Taniguchi T, Yang L, Xia F N 2020 Sci. Adv. 6 eaay6134

[44] Zhu L Q, Shao J, L ü X, Guo S L, Chu J H 2011 J. Appl. Phys. 109 013509

[45] Zhu L Q, Song Y, Qi Z, Wang S M, Zhu L Q, Chen X, Zha F X, Guo S L, Shao J H 2016 J. Lumin. 169 132

[46] Shao J, Qi Z, Zhao H, Zhu L Q, Song Y, Chen X R, Zha F X, Guo S L, Wang S M 2015 J. Appl. Phys. 118 165305

[47] Chen X R, Song Y, Zhu L Q, Wang S M, Lu W, Guo S L, Shao J 2013 J. Appl. Phys. 113 153505

[48] Dou C, Chen X R, Chen Q M, Song Y X, Ma N, Zhu L Q, Tan C S, Han L, Yu D G, Wang S M, Shao J 2022 Phys. Status Solidi B 259 2100418

[49] Yan B, Chen X R, Zhu L Q, et al. 2019 Appl. Phys. Lett. 114 052104

[50] Chen X R, Wu X Y, Yue L, Zhu L Q, Pan W W, Qi Z, Wang S M, Shao J 2017 Appl. Phys. Lett. 110 051903

[51] Chen X R, Zhao H, Wu X Y, Wang L, Zhu L Q, Song Y, Wang S M, Shao J 2019 Phys. Status Solidi B 256 1800694

[52] Zhu L Q, Shao J, Zhu L, Chen X R, Qi Z, Lin T, Bai W, Tang X D, Chu J H 2015 J. Appl. Phys. 118 045707

[53] Zhu L Q, Shao J, Chen X R, Li Y Q, Zhu L, Qi Z, Lin T, Bai W, Tang X D, Chu J H 2016 Phys. Rev. B 94 155201

[54] Chen X R, Zhuang Q, Alradhi H, Jin Z M, Zhu L Q, Chen X R, Shao J 2017 Nano Lett. 17 1545

[55] Chen X R, Zhou Y, Zhu L Q, Qi Z, Xu Q, Xu Z, Guo S L, Chen J X, He L, Shao J 2014 Jpn. J. Appl. Phys. 53 082201

[56] Chen X R, Xu Z C, Zhou Y, Zhu L Q, Chen J X, Shao J 2020 Appl. Phys. Lett. 117 081104

[57] Chen X R, Xing J, Zhu L Q, Zha F X, Niu Z, Guo S L, Shao J 2016 J. Appl. Phys. 119 175301

[58] Zhang X H, Shao J, Chen L, Lu X, Guo S L, He L, Chu J H 2011 J. Appl. Phys. 110 043503

[59] Shao J, Lu W, Tsen G K O, Guo S L, Dell J M 2012 J. Appl. Phys. 112 063512

[60] Zhu L Q, Liu S, Shao J, Chen X, Liu F, Hu Z, Chu J H 2023 Chin. Phys. Lett. 40 077503

[61] Zha F X, Shao J, Jiang J, Yang W Y 2007 Appl. Phys. Lett. 90 201112

[62] Zhang B P, Cai C F, Jin S Q, Ye Z Y, Wu H Z, Qi Z 2014 Appl. Phys. Lett. 105 022109

[63] Deng Z, Chen B L, Chen X R, Shao J, Gong Q, Liu H Y, Wu J 2018 Infrared Phys. Technol. 90 115

[64] Zhuang Q D, Alradhi H, Jin Z M, et al. 2017 Nanotechnol. 28 105710

[65] Huang J L, Ma W Q, Wei Y, Zhang Y H, Cui K, Cao Y L, Guo X L, Shao J 2012 IEEE J. Quant. Electron. 48 1322

[66] Xing J L, Zhang Y, Liao Y P, Wang J, Xiang W, Hao H Y, Xu Y Q, Niu Z C 2014 J. Appl. Phys. 116 123107

[67] Pan W W, Zhang L Y, Zhu L, Li Y Y, Chen X R, Wu X Y, Zhang F, Shao J, Wang S M 2016 J. Appl. Phys. 120 105702

[68] Chen Q M, Zhang L Y, Song Y X, et al. 2021 ACS Appl. Nano Mater. 4 897

[69] Xu Z C, Chen J X, Wang F F, Zhou Y, Jin C, He L 2014 J. Cryst. Growth 386 220

[70] Furstenberg R, White J O, Dinan J H, Olson G L 2004 J. Electron. Mater. 33 714

[71] Dyksik M, Motyka M, Sęk G, Misiewicz J, Dallner M, Weih R, Kam M, Höfling S 2015 Nanoscale Res. Lett. 10 402

[72] Pepper B, Soibel A, Ting D, Hill C, Khoshakhlagh A, Fisher A, Keo S, Gunapala S 2019 Infrared Phys. Technol. 99 64

[73] Kwan D C M, Kesaria M, Anyebe E A, Alshahrani D O, Delmas M, Liang B L, Huffaker D L 2021 Appl. Phys. Lett. 118 203102

[74] Chen X R, Zhu L Q, Shao J 2019 Rev. Sci. Instrum. 90 093106

[75] Chen X R, Zhu L Q, Zhang Y C, Zhang F, Wang S M, Shao J 2021 Phys. Rev. Appl. 15 044007

[76] Chen X R, Wang M, Zhu L Q, Xie H, Chen L, Shao J 2023 Appl. Phys. Lett. 123 151105

[77] Shi Z Y, Yan D Y, Zhang Y C, et al. 2023 J. Alloys Compounds 947 169410

[78] Chen X R, Shao J 2024 Rev. Sci. Instrum. 95 123906